



# Formation of Interstellar Complex Polycyclic Aromatic Hydrocarbons: Insights from Molecular Dynamics Simulations of Dehydrogenated Benzene

Meriem Hanine, Zhisen Meng, Shiru Lu, Peng Xie, Sylvain Picaud, Michel Devel, Zhao Wang

## ► To cite this version:

Meriem Hanine, Zhisen Meng, Shiru Lu, Peng Xie, Sylvain Picaud, et al.. Formation of Interstellar Complex Polycyclic Aromatic Hydrocarbons: Insights from Molecular Dynamics Simulations of Dehydrogenated Benzene. The Astrophysical Journal, 2020, 900 (2), pp.188. 10.3847/1538-4357/abab06 . hal-02989289

**HAL Id: hal-02989289**

**<https://hal.science/hal-02989289>**

Submitted on 5 Nov 2020

**HAL** is a multi-disciplinary open access archive for the deposit and dissemination of scientific research documents, whether they are published or not. The documents may come from teaching and research institutions in France or abroad, or from public or private research centers.

L'archive ouverte pluridisciplinaire **HAL**, est destinée au dépôt et à la diffusion de documents scientifiques de niveau recherche, publiés ou non, émanant des établissements d'enseignement et de recherche français ou étrangers, des laboratoires publics ou privés.

Formation of interstellar complex polycyclic aromatic hydrocarbons: Insights from molecular dynamics simulations of dehydrogenated benzene

MERIEH HANINE,<sup>1</sup> ZHISEN MENG,<sup>1</sup> SHIRU LU,<sup>1</sup> PENG XIE,<sup>2</sup> SYLVAIN PICAUD,<sup>3</sup> MICHEL DEVEL,<sup>4</sup> AND ZHAO WANG<sup>1,5</sup>

<sup>1</sup>*Laboratory for Relativistic Astrophysics, Department of Physics, Guangxi University, 530004 Nanning, China*

<sup>2</sup>*School of Chemistry and Chemical Engineering, Guangxi University, 530004 Nanning, China*

<sup>3</sup>*Observatoire de Besançon, Institut UTINAM, CNRS UMR 6213, UBFC, 25030 Besançon, France*

<sup>4</sup>*FEMTO-ST institute, CNRS, ENSMM, 15B avenue des Montboucons, 25030 Besançon, France*

<sup>5</sup>*Institute of Materials Chemistry, TU Wien, 1060 Vienna, Austria*

(Received ; Revised ; Accepted )

Submitted to ApJ

## ABSTRACT

Small organic molecules are thought to provide building blocks for the formation of complex interstellar polycyclic aromatic hydrocarbons (PAHs). However, the underlying chemical mechanisms remain unclear, particularly concerning the role of interstellar dust. Using molecular dynamics, we simulate the chemical reaction between dehydrogenated benzene molecules in the gas phase or on the surface of an onion-like carbon nanoparticle (NP). The reaction leads to the formation of PAHs of complex structures. The size of the formed molecules is found to roughly increase at increasing temperature up to 800 K, and to be correlated with the level of dehydrogenation. Morphology analysis features the formation of large rings that contain up to 32 carbon atom at high temperature. Density functional theory (DFT) calculations are performed to search the fundamental energetic reaction pathways. The DFT results quantitatively confirm the correlation between the reactivity and the dehydrogenation level, and the formation of stable C-8 rings. Moreover, the layered nanostructures formed on the NP surface point to a possible layer-by-layer formation mechanism for interstellar fullerene and carbon onions.

**Keywords:** Astrochemistry (75), Polycyclic aromatic hydrocarbons (1280), Interstellar molecules (849), Molecule formation (2076), Interstellar medium (847)

## 1. INTRODUCTION

Polycyclic aromatic hydrocarbons (PAHs) are among the most studied molecules in the fields of chemistry, astronomy, biology and environmental science (Keyte et al. 2013). PAHs are found to be highly abundant in the interstellar medium (ISM), and to play important roles in its evolution

(Tielens 2008). Small interstellar organic molecules have been hypothesized to be involved in the formation of complex PAHs, which in turn are believed to be building blocks of complex organic molecules (Ehrenfreund et al. 2006; Rapacioli et al. 2006; Ehrenfreund & Charnley 2000). The building sequence could be crucial in explanations of ISM evolution and abiogenesis (Wakelam & Herbst 2008; Galliano & Dwek 2008; Kim et al. 2012; Sandstrom et al. 2012; Puzzarini et al. 2017). However, the underlying physicochemical mechanisms of the formation process of large and complex PAHs remain unclear, particularly regarding the key stage of chemical reactions between small organic compounds involving interstellar dust.

Recent space- and ground-based observations via infrared radiation (IR) spectroscopy have revealed the abundance of diverse carbon nanostructures in the interstellar dust, including fullerene, diamond, graphite, soot, and so forth (Li et al. 2019; Bernal et al. 2019; Zhang & Kwok 2011; Boi et al. 2017). They were reported to co-exist with PAHs in various regions of ISM and likely to influence the chemical evolution of PAHs (Cami et al. 2010; García-Hernández et al. 2010; Chhowalla et al. 2003). In one of our recent works, we have studied the interaction between adsorbed organic molecules on a fullerene-like carbon onion by means of classical molecular dynamics (MD) simulations (Qi et al. 2018). Calculations of molecular binding energy have suggested that carbon nanostructures could provide substrates for forming molecular layers and aggregations. However, the chemical reaction remains unexplored since we only studied fully saturated molecules.

From a chemical perspective, high energy barrier is expected for the interaction between fully hydrogenated PAHs (Chen 2018). Photofragmentation involving the dehydrogenation in ISM regions with strong UV irradiation is thus considered as the main mechanism leading to the formation of new PAH species. For instance, Castellanos et al. have demonstrated that the balance between H-loss due to UV irradiation and reactions with atomic H shifts towards gaseous dehydrogenated PAHs. The existence of dehydrogenated PAHs in ISM has also been suggested by Mackie et al. based on numerical analysis of Spitzer IR emission spectra (Mackie et al. 2015). A recent laboratory study has reported the formation of large PAHs following photodissociation and photodehydrogenation processes of PAH clusters (Zhen et al. 2018). In light of these evidences, we study chemical reaction between unsaturated organic molecules using MD based on a reactive force field, in order to gain insights into the formation of large and complex structures of PAHs. These simulations are performed for dehydrogenated benzene either in the gas phase or on a carbon onion-like nanoparticle (NP) (Boi et al. 2017; Krasnokutski et al. 2017). Density functional theory (DFT) calculations were also performed to identify fundamental reaction pathways. We explore the complex structures of the formed PAHs by means of morphology analyses.

## 2. METHODS

It is known that dehydrogenation can occur in ISM environments through irradiation with, for instance, cosmic rays or ultraviolet (UV) photons (Piani et al. 2017), as evidenced by the discovery of unsaturated molecules in ISM (Herbst & van Dishoeck 2009; Mackie et al. 2015). Even slight dehydrogenation could make molecules highly reactive (Chen 2018; Petrignani et al. 2016; Krasnokutski et al. 2017). To simulate the formation of PAHs, we here take the smallest aromatic unit, benzene, with different levels of dehydrogenation ( $C_6H_5$ ,  $C_6H_4$ ,  $C_6H_2$  and  $C_6H_1$ ) as the samples shown in Figure 1 (a). The carbon NP is modeled by a bucky-onion containing several concentric fullerene layers (Langlet et al. 2007) as shown in Figure 1 (b), in order to mimic the onion-like nanostructures observed in transmission electron microscopy experiments (Krasnokutski et al. 2017; Rotundi et al.

1998; Jäger et al. 2006, 2009). This model is in general consistent with the previously-reported low H/C ratio and high aromaticity of the galactic hydrocarbon dust (Chiar et al. 2013).

In our MD model, the interatomic interaction is described by a many-body force field, the adaptive interatomic reactive empirical bond order (AIREBO) model, which enables the formation or the breaking of chemical bonds using a spline-smoothed transition from long-range van der Waals (vdW) interaction to covalent bonding, or viceversa. Details of this force field, including its formulation, parameter values and benchmark calculations are provided in Stuart et al. (2000). This force field has been widely used for simulating  $sp^2$  hydrocarbons, and has shown reasonable accuracy in modeling chemical reaction, see e.g. Liu & Stuart (2011).

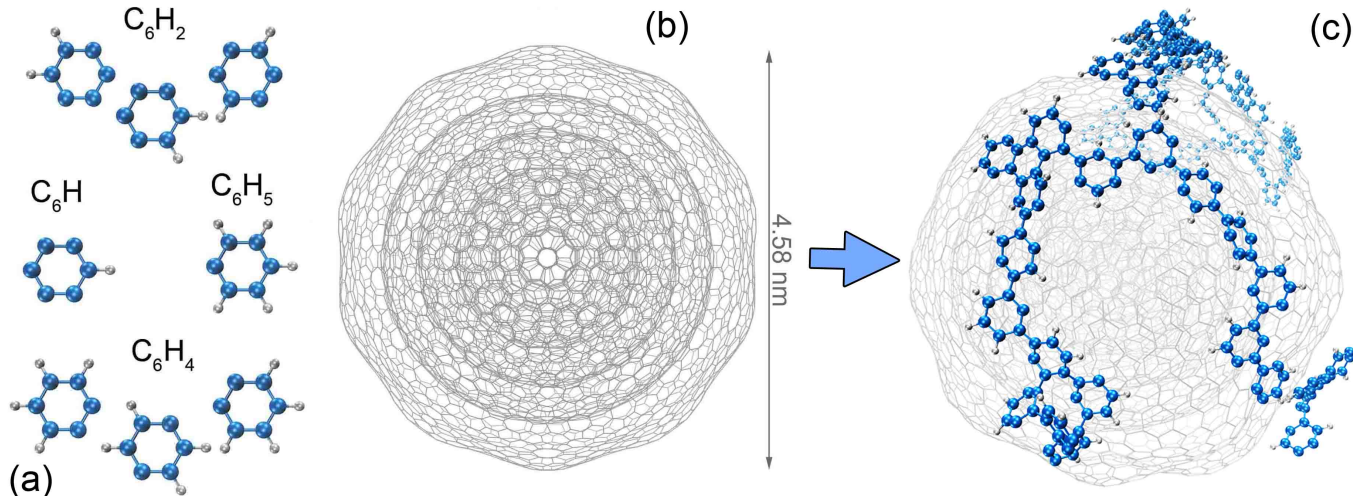


**Figure 1.** (a) Ball-and-stick model of the dehydrogenated organic compounds studied in this work. Carbon atoms are depicted in blue, hydrogens in gray. (b) Line model of the onion-like fullerene structure of the carbon NP (diameter = 4.58 nm). (c) Snapshot of the simulation cell that contains PAH molecules formed on the NP from  $C_6H_2$  at 300K.

A periodic simulation box (about  $10 \times 10 \times 10 \text{ nm}^3$  in size) is prepared, in which 60 organic molecules and a carbon NP are placed at random sites in vicinity. The parallel computing package LAMMPS was used (Plimpton 1995) for the MD simulations. After initial velocities are randomly assigned to each atoms, the NP is brought to thermal equilibrium by a Nosé-Hoover thermostat. Note that adsorption of most of the organic molecules occurs on the NP surface during equilibration, where these molecules can start to form new species through chemical reactions. The cases of the gas phase (without NP) are also simulated. Since the temperature of ISM can vary a lot in different environments (Ferrière 2001; Zheng et al. 2008; Pino et al. 2019; Fu et al. 2012), we simulate the reaction between the organic molecule at different temperatures, including 10, 100, 200, 300, 600, 800 and 1000 K, in order to gain insight on the temperature dependence. With a time step of 0.5 fs, the duration of every simulation is set to be 4.0 ns (i.e. 8,000,000 steps) according to the maximum of our computational resource. Despite the radical density will be much lower in space (Elmegreen 2007), the molecular density is here set to be high enough in order to speed up the reaction simulation for the sake of calculability, by considering that many collisions will occur over time.

### 3. RESULTS AND DISCUSSIONS

## 3.1. Statistical distribution

PAH molecules of different topology are observed to form as shown in Figure 1 (c) for example. The atomistic configurations of the formed molecules are recorded at different instance during the simulations. It is observed that small molecules spontaneously bind to each other to form small PAHs, which further cluster to form large and complex structures. In contrast to  $C_6H_2$  and  $C_6H$ ,  $C_6H_5$  and  $C_6H_4$  only produces small PAHs such as diphenyls. We therefore focus on the complex structures of PAHs formed from  $C_6H$  and  $C_6H_2$  in the following discussion. Note that detailed reaction sequences are illustrated via animations provided in APPENDIX A.

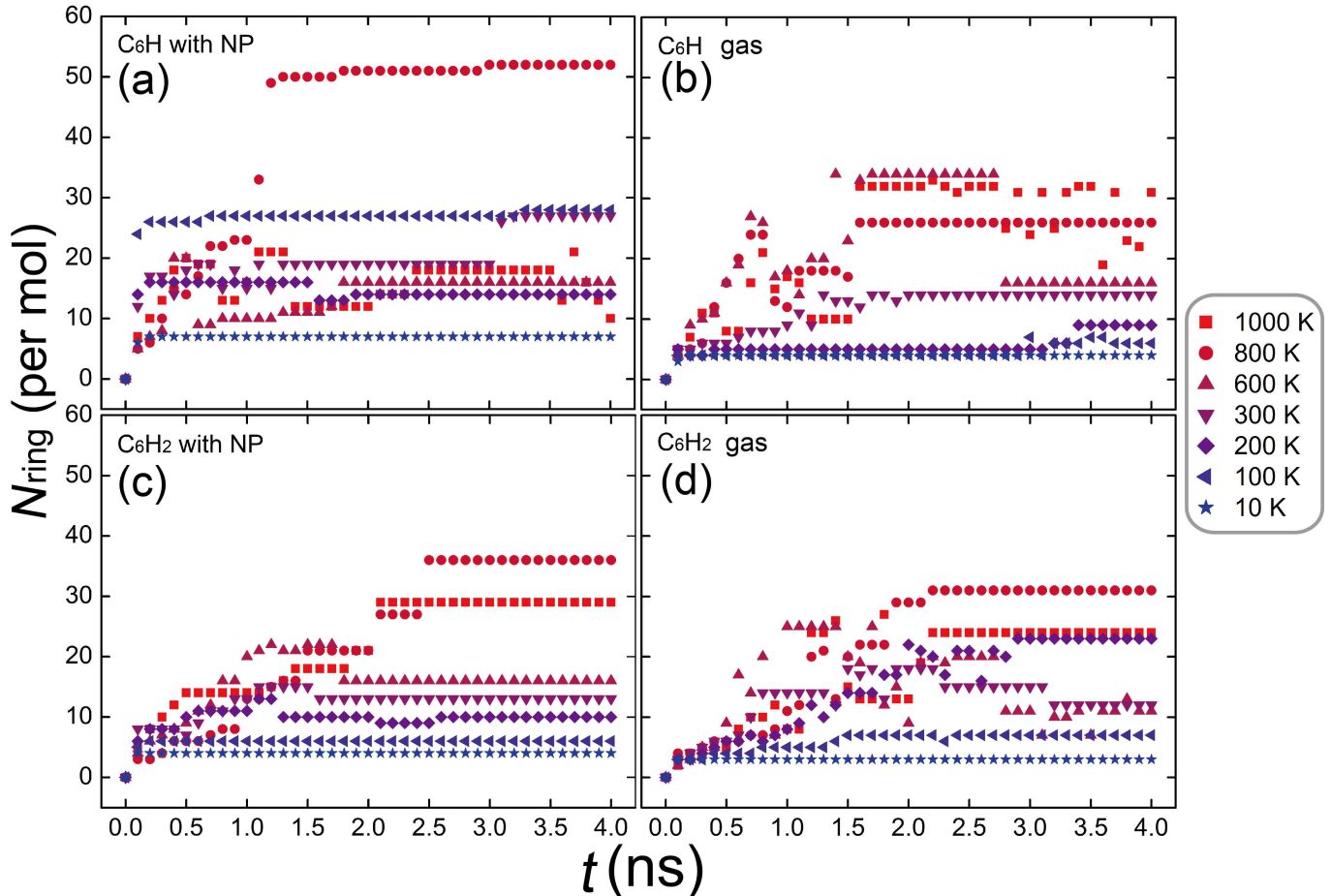


**Figure 2.** Number of carbon rings  $N_{ring}$  in the formed PAH molecules vs the simulation time  $t$  for  $C_6H$  and  $C_6H_2$  at different temperatures on the NP surface (a,c) or in the gas phase (b,d). The per-molecule value of  $N_{ring}$  is averaged over all formed molecules in a simulation cell.

To measure the size of the complex structures, we compute the number of carbon rings  $N_{ring}$  in each formed PAH molecule. Figure 2 shows the time-evolution of the averaged per-molecule value of  $N_{ring}$  for  $C_6H$  (top panels) or  $C_6H_2$  (bottom panels) at various temperatures. It is seen that the PAH size roughly increases with increasing temperature. This trend is notably kept in the cases of  $C_6H$  in the gas phase (panel b) and of  $C_6H_2$  on the NP surface (panel c) at up to 800 K. Figure 2 also shows a difference in the reactivity due to different levels of dehydrogenation, as the PAHs formed from  $C_6H$  (upper panels) are in general larger than those formed from  $C_6H_2$  (lower panels). Moreover, the



averaged size of the PAHs formed on the NP (left panels) seems to be slightly larger than that of the ones formed in the gas phase (right panels) at most of the temperatures studied here.

At low temperature, the nucleation of the PAH is hampered by slow diffusion and low collision rate, which result in saturated curves of  $N_{ring}$  (horizontal lines in Figure 2). In contrast, the size of formed molecules varies frequently at high temperatures, in particular at 1000 K. This signifies the breaking or the merging of carbon rings, and thus indicate a possible change in the formation mechanism. Among the studied temperatures, the optimized temperature for forming large and stable PAH structures is 800 K, for both the cases in the gas phase and on the NP. Note that Marshall and Sadeghpour have also shown by MD simulations that the formation of chain- or fullerene-like molecules is faster at 100 – 500 K on a graphene surface than in the gas phase, but it becomes slower above 1000 K (Marshall & Sadeghpour 2016).

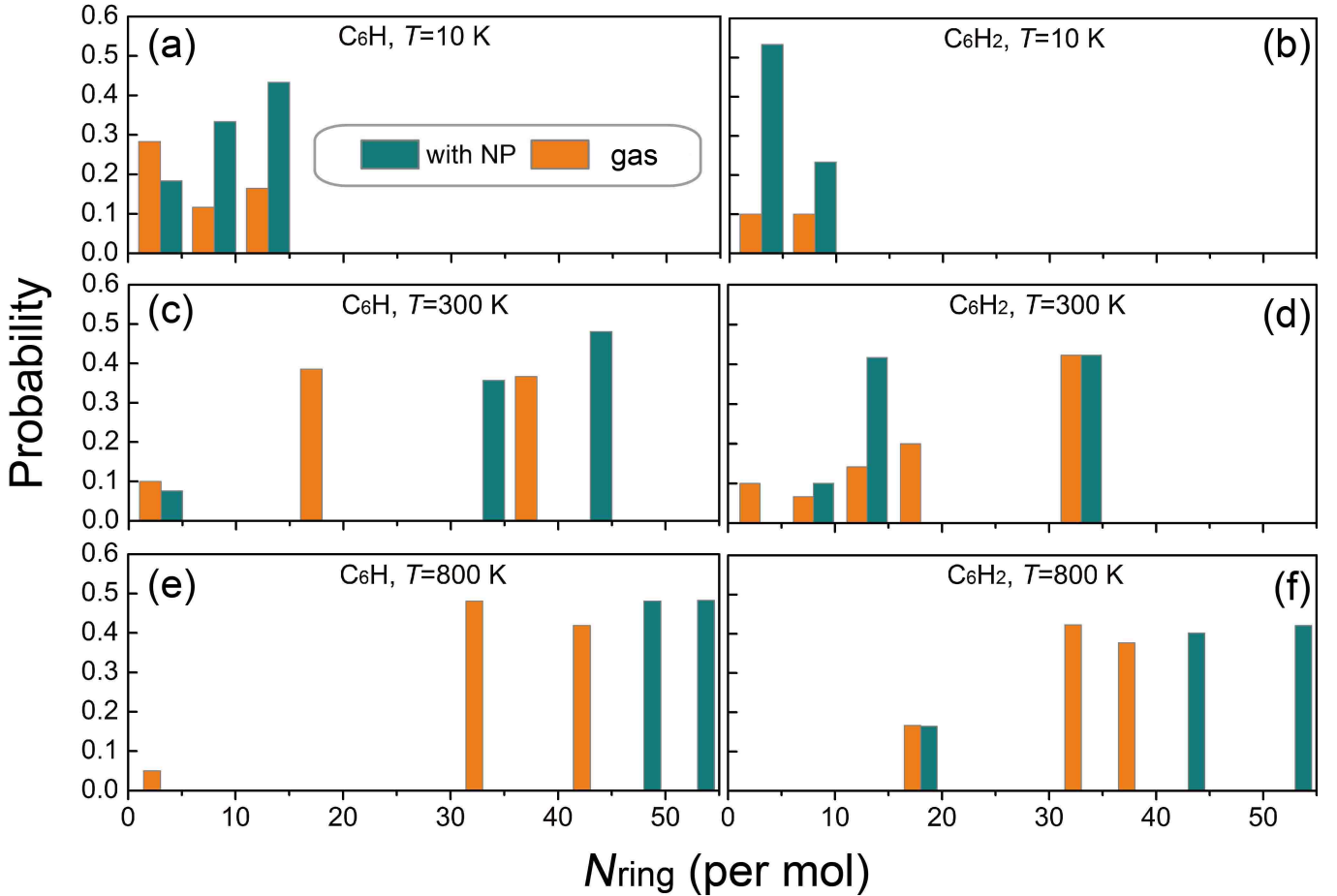


**Figure 3.** Probability distribution of PAH molecules formed from  $C_6H$  (left panels) or  $C_6H_2$  (right panels) at (a,b) 10, (c,d) 300, (e,f) 800 K. The probability is calculated to be the ratio between the number of atoms in the formed molecule over the total number of the atoms in the simulation cell.

The PAHs formed on the NP surface are found to be slightly larger than those formed in the gas phase. This effect can be more clearly seen within the plot of the probability distribution of the averaged carbon rings in Figure 3, which shows that large PAH molecules form more efficiently in presence of the NP. It can also be seen that the sum of probability is much smaller than 1.0 for the

low-temperature (10 K) case in the gas phase. This signifies that many of the benzene molecules do not participate the reaction of PAH synthesis due to their low mobility despite of the high molecular density.

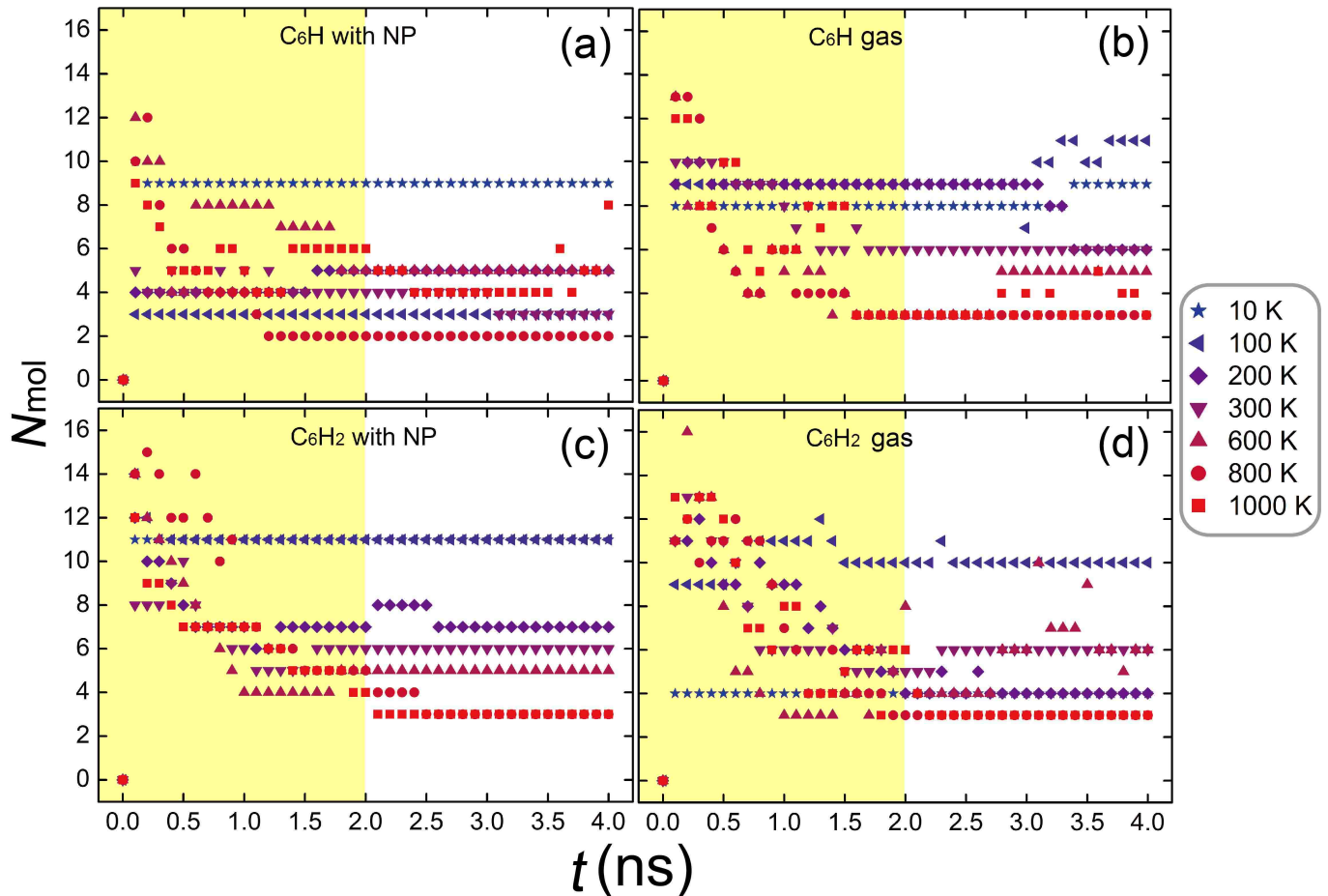


**Figure 4.** Time-evolution of the number of the PAH molecules formed in the simulation cells.

One may wonder whether the PAH structures formed in 4.0 ns will be the final products. To answer this question, we plot in Figure 4 the number of formed PAH molecules  $N_{mol}$  as a function of the simulation time. It is seen that the evolution of  $N_{mol}$  strongly depends on the applied temperature. For our simulation model, most of the reactions seem to take place within the first 2.0 ns (highlighted by the colored zone). Further isomerization keeps taking place on a longer timescale with however much lower rate, in particular in the gas phase. At the optimized temperature of 800 K that leads to large PAHs, the reaction seems to be possibly finalized within 2.5 ns for all the four considered cases.

### 3.2. Morphology analysis

In this section, we investigate the temperature effect on the PAH formation by analyzing the detailed morphology of the formed molecular structures. Figure 5 shows the growth of the PAHs formed on the NP surface over time from  $C_6H$  at four different temperatures. In keeping with the statistics shown in the previous section, the molecular structures formed at low temperature do not

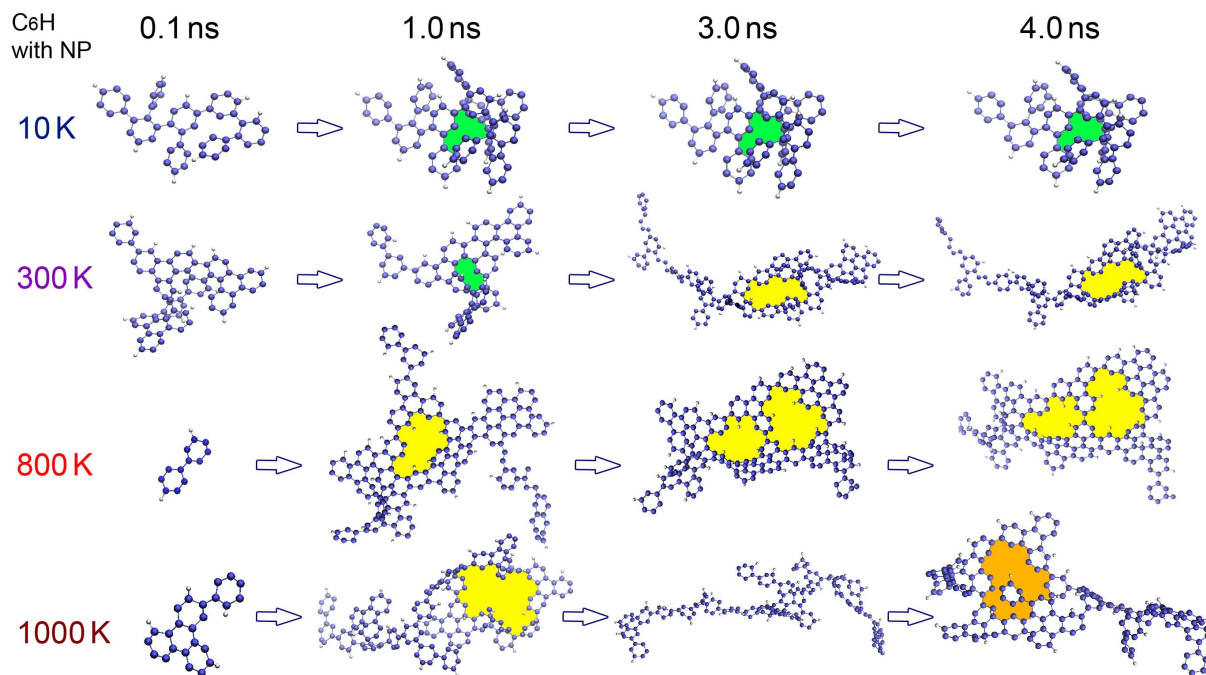


**Figure 5.** Time-evolution of the morphology of PAH molecules formed from C<sub>6</sub>H on the NP (not shown) at different temperatures.

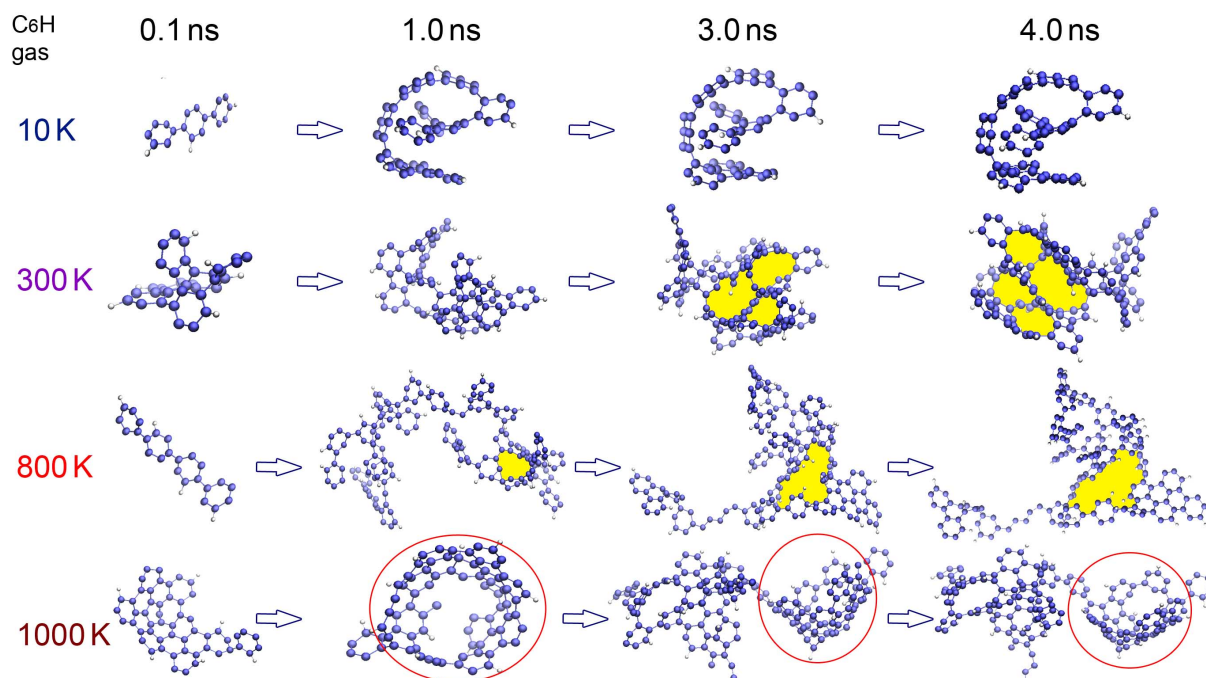


**Figure 6.** Time-evolution of the morphology of PAH molecules formed from C<sub>6</sub>H in gas phase at different temperatures.



significantly change in the nanosecond time scale, but can vary a lot at high temperatures. The formation of large carbon rings are highlighted by the colored patterns in Figure 5. These large rings seem to maintain the connectivity of the typical  $sp^2$  lattice in PAHs (and in fullerene) chaining more than 6 carbon atoms. These large C-rings efficiently form at high temperatures, while their sizes change over time. For instance at 1000 K, a large C-ring is formed in 1.0 ns by the collisions between small molecules, it then breaks in the following 2.0 ns, before a new large C-ring is formed in 4.0 ns by connecting suspended carbon chains.

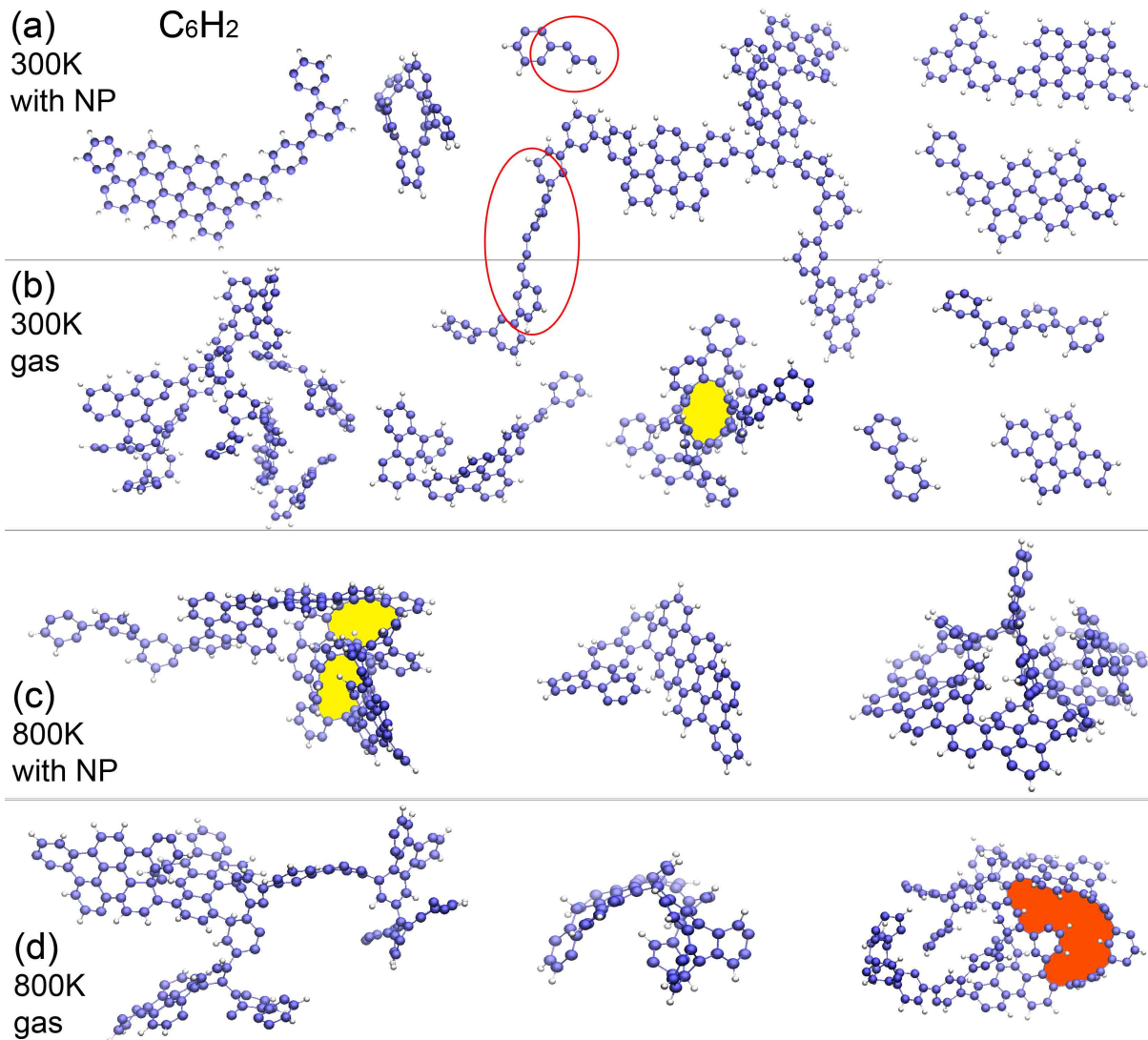


**Figure 7.** Morphology of PAH molecules formed from 60  $C_6H_2$  molecules at 300 and 800 K in 4.0 ns.

It has long been recognized (by the so-called Mermin-Wagner theorem) that two-dimensional (2D) structures embedded in a 3D space have a tendency to be crumpled, since long-wave length fluctuations destroy the long-range order of 2D crystals (Nelson et al. 2004). It is seen in Figure 5 that most of the molecules formed on the NP are flatter than those formed in the gas phase, thanks to the supporting substrate. In contrast, the molecules formed in the gas phase are mostly curved, as shown in Figure 6. This observation, together with aforementioned large PAHs formed on the NP

surface (Figure 3), point to a possible layer-by-layer formation mechanism of fullerene and carbon onions, which have been reported to co-exist with PAHs in ISM (Cami et al. 2010; García-Hernández et al. 2010; Chhowalla et al. 2003; Zhang & Kwok 2011).

An *e*-shaped molecule is formed at 10K by rolling up a flat PAHs. We have performed structural optimization for this particular molecule by minimizing its potential energy, and found this curled structure is quite stable at a local potential minimum. Similar to the case on the NP, large carbon rings can also form in the gas phase as highlighted by the colored patterns, in particular at high temperature. Interestingly, a tubular structure is observed to form at 1000 K in 1.0 ns, as shown in the circles in Figure 6. This tube-like molecule transforms into a cap-like structure in 3.0 ns. This is in line with the simulations of Sadeghpour et al., in which curved cage-like carbon nanostructures were observed to form (Marshall & Sadeghpour 2016; Patra et al. 2014).

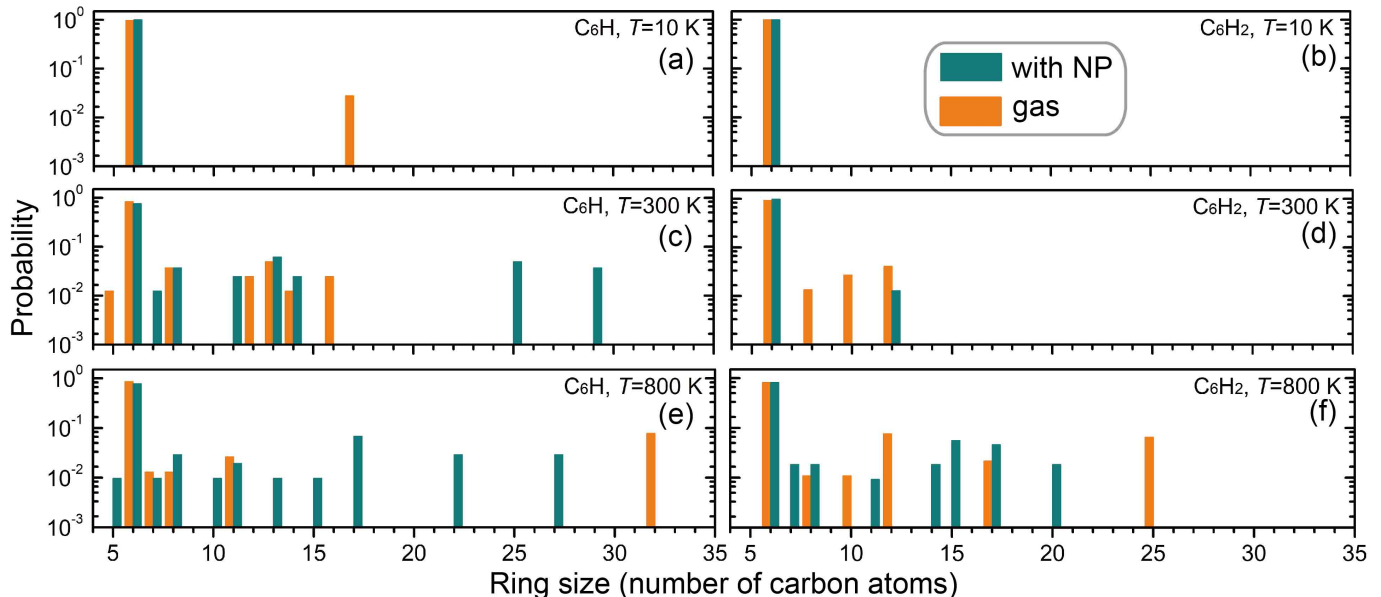


**Figure 8.** Probability distribution of the number of carbon atoms in the rings of the PAH molecules formed from  $C_6H$  (left panels) or  $C_6H_2$  (right panels) at (a,b) 10, (c,d) 300, (e,f) 800 K. The probability is calculated as the ratio between the numbers of rings of a given size over the total number of rings of all formed molecules in a simulation cell.

Figure 7 shows the structures of molecules formed from  $C_6H_2$  in 4.0 ns. Similar to  $C_6H$ , it can be seen that the PAH molecules formed in the gas phase are in general more crumpled than those formed on the NP, except for the small ones. We also observe large carbon rings as well as mono-atomic chains (as shown in the red circles). The formation of these chains implies the breaking of carbon rings in the source molecules, the structural instability of which is probably induced by dehydrogenation. A very large C-ring chaining 27 carbon atoms (highlighted by the red pattern) is observed at 800 K in the gas phase. Moreover, we note that many of the sub-structures of these formed molecules are similar to those of the PAHs collected in the NASA AMES PAH IR spectroscopic database (Bauschlicher et al. 2018). We note that the molecular structures shown in this section only include a small portion of the PAH molecules formed in our simulations. A complete set of the structures of all new PAH molecules formed under different conditions are provided in APPENDIX B.

Figure 8 provides statistics on the ring size of the PAHs formed in 4.0 ns. It is seen that the probability for producing large carbon rings increases with increasing temperatures. This probability is in general higher for  $C_6H$  than for  $C_6H_2$ . Most of these rings contain less than 17 carbon atoms, including a number of pentagonal carbon (C-5) rings formed (e.g. from  $C_6H$ ). Remarkably, a very large ring containing 32 carbon atoms is formed at 800 K from  $C_6H$  in the gas phase. We note that octagonal carbon (C-8) rings present in all the cases at 300 and 800 K for both  $C_6H$  and  $C_6H_2$  in the gas phase and on the NP.

### 3.3. DFT-calculated reaction pathways

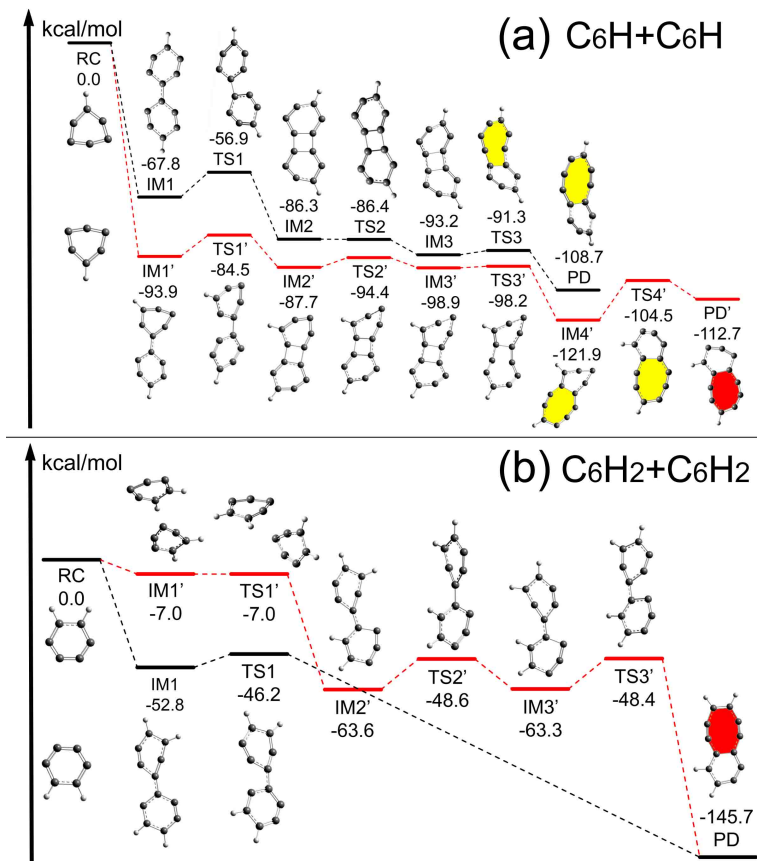


**Figure 9.** DFT-computed free-energy diagram for the reaction between a pair of molecules of (a)  $C_6H_2$  or (b)  $C_6H$ . The most energy-favorable reaction mechanism is highlighted in black color, while the second favorable one is in gray. All energy values are the Gibbs free energies at 15 K in the unit of kcal/mol. Details on the optimized structures and their atomic coordinates are provided in APPENDIX C.

To complement our MD simulations, first-principles DFT calculations are carried out to investigate the detailed chemical reaction pathway between individual pairs of molecules in single collision events at the atomistic level. The resulting molecular structures in the collision are optimized using the M06 functional (Zhao & Truhlar 2008) with 6-31+g(d, p) basis sets as implemented in Gaussian 16 B.01 (Frisch et al. 2016). Frequency calculations are also performed to confirm the intermediate (IM) or transition (TS) states). In addition, intrinsic reaction coordinate (IRC) calculations are carried out to make sure that TS actually connects the reasonable reactant (RC) and product (PD). Multiple

(typically 8 – 10) possible initial collision positions are considered for each pair of molecules, leading to multiple reaction pathways, among which the most energetically-favorable ones are selected and shown by the red lines in Figure 9.

All of these reactions are exothermic and roughly barrierless. The energy released in the first step seems to be large enough to overcome all the subsequent energy barriers if the radiation loss is considerable. This indicates that even at temperatures as low as 10 – 20 K in cold molecular clouds, these reactions can always occur due to the high chemical reactivity of unsaturated molecules. This is in agreement with [Parker et al. \(2015\)](#), who have studied the formation of nitrogen-substituted PAHs. Furthermore, the large energy difference between the RC and the PD states implies there will be a high enthalpy released from chemical reaction to the kinetic energy of the formed molecule. In an interstellar environment with very low molecular density, this would suggest that the chemical reaction between PAHs could induce strong infrared emission signals, including even those from unstable intermediate or transitional molecular structures.

DFT calculations confirm the formation of PAHs containing stable C-8 rings through a serial of quasi-barrierless processes. It is found that the reaction between two  $C_6H_5$  is the simplest, which needs direct collision between the reaction sites and it releases an amount of energy as large as 160.1 kcal/mol. Figures 9 (a-b) show that the reactions between  $C_6H_2$  or  $C_6H$  lead to formation of octagonal carbon rings (C-8). The energy barrier is 10.9 kcal/mol for two  $C_6H$  and 6.6 kcal/mol for two  $C_6H_2$ . When two radical monomers get close to each other, a covalent bond would be formed with releasing amounts of heat (-67.8 kcal/mol for  $C_6H+C_6H$  and -52.8 kcal/mol for  $C_6H_2+C_6H_2$ ). The highest energy barriers along the most energetically-favorable reaction path are 10.9 and 6.6 kcal/mol when considering two  $C_6H$  and two  $C_6H_2$ , respectively.

#### 4. CONCLUSION

MD simulations suggest that the reaction between dehydrogenated benzene molecules can lead to the formation of complex PAH structures. The size of the PAH molecules roughly increases with increasing temperature in the gas phase or on the NP. An optimized temperature at the order of 800 K is revealed in favor of forming large-size PAHs. The PAH size is also positively correlated with the level of dehydrogenation. Morphology analysis reveals the formation of large rings that contain more than 6 carbon atoms. The probability for producing the large rings increases with increasing temperatures, and is in general higher for  $C_6H$  than for  $C_6H_2$ . DFT calculations identify the most possible reaction pathways, and quantitatively confirm the difference in the reactivity between  $C_6H$  and  $C_6H_2$ , as well as the formation of stable C-8 rings. We also observe the formation of (unstable) mono-atomic chains, as well as tubular and cap-like nanostructures. There is a general trend to form layered nanostructures of relatively large size on the NP surface, which points to a possible layer-by-layer formation mechanism for interstellar fullerene and carbon onions.

J. Carrete, G. K. H. Madsen, P. Blaha and K. Schwarz are acknowledged for helpful discussions. We note that M. Hanine, Z. Meng and S. Lu equally contributed to this work. Partial financial support from the National Natural Science Foundation of China (11964002), Guangxi Science Foundation

(2018GXNSFAA138179), Guangxi Key Laboratory Foundation (15-140-54) and Scientific Research Foundation of Guangxi University (XTZ160532) is acknowledged.

## APPENDIX

### A. ANIMATIONS OF THE FORMATION PROCESS

The video/animations demonstrating the formation process of PAH are available on the AAS website.

### B. ATOMISTIC CONFIGURATIONS OF FORMED PAHS

Atomistic configurations of the formed PAH molecules (in 4.0 ns) at all studied temperatures are available in .xyz format on the AAS website. These .xyz files contain the atomic coordinates of the formed molecules by giving the total number of atoms that will be read on the first line; the comment text on the second; and the atomic number and three atomic Cartesian coordinates in the following lines. The name of the .xyz file consists of four parts separated by “\_” including the source molecule type, the temperature, the formation environment (with NP or in gas phase), and the molecular ID (among multiple molecules formed in a simulation). For instance, “C6H2\_300K\_gas\_2.xyz” stands for the 2nd molecule formed from C<sub>6</sub>H a2t 300 K in the gas phase.

### C. DFT-COMPUTED ATOMISTIC COORDINATE DATA FILES

A data file that contains the DFT-calculated optimized structures and their atomic coordinates is provided on the AAS website.

## REFERENCES

- Bauschlicher, C. W. J., Ricca, A., Boersma, C., & Allamandola, L. J. 2018, *ApJS*, 234, 32
- Bernal, J. J., Haenecour, P., Howe, J., et al. 2019, *ApJL*, 883, L43
- Boi, F. S., Zhang, X. T., Ivaturi, S., et al. 2017, *JAP*, 122, 224305
- Cami, J., Bernard-Salas, J., Peeters, E., & Malek, S. E. 2010, *Sci*, 329, 1180
- Chen, T. 2018, *ApJ*, 866, 113
- Chhowalla, M., Wang, H., Sano, N., et al. 2003, *PhRvL*, 90, 155504
- Chiar, J. E., Tielens, A. G. G. M., Adamson, A. J., & Ricca, A. 2013, *ApJ*, 770, 78
- Ehrenfreund, P., & Charnley, S. B. 2000, *ARA&A*, 38, 427
- Ehrenfreund, P., Rasmussen, S., Cleaves, J., & Chen, J. 2006, *AsBio*, 6, 490
- Elmegreen, D. M. 2007, *ApJ*, 668, 1064
- Ferrière, K. M. 2001, *RvMP*, 73, 1031
- Frisch, M. J., Trucks, G. W., Schlegel, H. B., & et al. 2016, Gaussian, 16 revision B.01. Gaussian Inc.: Wallingford, CT, USA
- Fu, Y., Szczepanski, J., & Polfer, N. C. 2012, *ApJ*, 744, 61
- Galliano, F., & Dwek, E. 2008, *ApJ*, 672, 214
- García-Hernández, D. A., Manchado, A., García-Lario, P., et al. 2010, *ApJL*, 724, L39
- Herbst, E., & van Dishoeck, E. F. 2009, *ARA&A*, 47, 427
- Jäger, C., Huiskens, F., Mutschke, H., Jansa, I. L., & Henning, T. 2009, *ApJ*, 696, 706
- Jäger, C., Krasnokutski, S., Staicu, A., et al. 2006, *ApJS*, 166, 557
- Keyte, I. J., Harrison, R. M., & Lammel, G. 2013, *ChSocRv*, 42, 9333
- Kim, J. H., Im, M., Lee, H. M., et al. 2012, *ApJ*, 760, 120
- Krasnokutski, S. A., Goulart, M., Gordon, E. B., et al. 2017, *ApJ*, 847, 89
- Langlet, R., Mayer, A., Geuquet, N., et al. 2007, *Physics, Chemistry and Application of Nanostructures*, ed. V. E. Borisenko, V. S. Gurin, & S. V. Gaponenko (Singapore)



- Li, Q., Li, A., & Jiang, B. W. 2019, *MNRAS*, 490, 3875
- Liu, A., & Stuart, S. J. 2011, *JCoCh*, 29, 601
- Mackie, C. J., Peeters, E., Bauschlicher, C. W., & Cami, J. 2015, *ApJ*, 799, 131
- Marshall, D. W., & Sadeghpour, H. R. 2016, *MNRAS*, 455, 2889
- Nelson, D. R., Piran, T., & Weinberg, S., eds. 2004, *Statistical Mechanics of Membranes and Surfaces* (World Scientific, Singapore)
- Parker, D. S. N., Yang, T., Dangi, B. B., et al. 2015, *ApJ*, 815, 115
- Patra, N., Kral, P., & Sadeghpour, H. R. 2014, *ApJ*, 785, 6
- Petrignani, A., Vala, M., Eyler, J. R., et al. 2016, *ApJ*, 826, 33
- Piani, L., Tachibana, S., Hama, T., et al. 2017, *ApJ*, 837, 35
- Pino, T., Chabot, M., Béroff, K., et al. 2019, *A&A*, 623, A134
- Plimpton, S. 1995, *JCoPh*, 117, 1
- Puzzarini, C., Baiardi, A., Bloino, J., et al. 2017, *ApJ*, 154, 82
- Qi, H., Picaud, S., Devel, M., Liang, E., & Wang, Z. 2018, *ApJ*, 867, 133
- Rapacioli, M., Calvo, F., Joblin, C., et al. 2006, *A&A*, 460, 519
- Rotundi, A., Rietmeijer, F. J. M., Colangeli, L., et al. 1998, *A&A*, 329, 1087
- Sandstrom, K. M., Bolatto, A. D., Bot, C., et al. 2012, *ApJ*, 744, 20
- Stuart, S. J., Tutein, A. B., & Harrison, J. A. 2000, *JChPh*, 112, 6472
- Tielens, A. G. G. M. 2008, *ARA&A*, 46, 289
- Wakelam, V., & Herbst, E. 2008, *ApJ*, 680, 371
- Zhang, Y., & Kwok, S. 2011, *ApJ*, 730, 126
- Zhao, Y., & Truhlar, D. G. 2008, *TCAcc*, 120, 215
- Zhen, J., Chen, T., & Tielens, A. G. G. M. 2018, *ApJ*, 863, 128
- Zheng, W., Jewitt, D., Osamura, Y., & Kaiser, R. I. 2008, *ApJ*, 674, 1242